Rotating flow instability inception prediction via eigen-analysis

Shenren Xu *[1], Chen He[2], and Dingxi Wang[1]
[1]*Northwestern Polytechnical University, Xi'an 710072, People's Republic of China*
[2]*Beihang University, Beijing 100191, People's Republic of China*

The compression system in turbomachines, e.g., aircraft engines and gas turbines, when operating under off-design conditions, exhibits self-excited unsteady phenomena such as surge, rotating stall and rotating instability, leading to performance deterioration and/or structural damages. Inability to accurately predict when such flow instability occurs limits the development of high performance compression system. Conventional methods for predicting the onset of such instabilities include analytical, semi-analytical-semi-emperical, and unsteady computational fluid dynamics (CFD) simulation, which are either fast but less accurate, or more accurate but requires long computational time. For engineering application, only steady state CFD analyses are affordable for deployment in practicla workflow. In this paper, we explore using the eigenanalysis approach to predict the onset of such instabilities. The key benifit of such analysis is that it is capable to capture exactly the eigenmodes that destabilize with computational cost of a few steady analyses. Pivotal to such analysis is a robust steady state RANS flow solver using the Newton–Krylov time-integration scheme which explicitly forms the Jacobian matrix. Once the flow has converged fully, the Jacobian matrix is used to compute the relavent eigenvalues and vectors. The methodology is applied to the computation of stability boundary of (i) the laminar flow around a two-dimensional circular cylinder, and (ii) the flow around a quasi-three-dimensional compressor anuular cascade. The method developed here has the potential to revive the once-popular eigenvalue method for prediction rotating stall and surge, and to provide industry with tools to accurately predict the stall line in the early design stage.

I. Todo list

- Investigate the fouriour spectrum of the circumferential signal of the eigenvectors and interpret the various frequency components. Why ND=5, 17?
- Compare unstable modes with URANS.

*Corresponding author, email address: shenren_xu@nwpu.edu.cn

II. Introduction

Rotating stall and rotating instability has been studied extensively both experimentally and numerically. Early experimental work revealed the basic features of such phenemenon and subsequent work has focused on the modelling of such phenomenon using simple analytical models. Simple analytical methods have had their success in the early days but the cost remaims prohibitively high when applied to realistic configurations and more detail is needed for quantitative prediction of the stall behavior.

However, previous numerical investigations mainly focused on using time-dependent unsteady flow analysis using either a fraction or the whole of an annulus. A lot of insight into the flow physics for the destablization mechanism has been gained using such high fidelity simuation approaches. Unsteasy simulation is useful for both reproducing the fully destabilized unsteady flows as well as for studying the inception of such instability.

Due to the high computatioal cost of unsteady simulation, it still remains largely as a reserach tool to investigate the stall phenomenon on a case-by-case basis and the cost is too high to apply it to daily design work and use it routinely.

Eigenvalue analysis is a powerful yet inexpensive tool to probe the flow near the critical condition, revealing rich flow physics with cost comparable to a steady state analysis. In this work, we demonstrate that using eigenvalue analysis based on a whole-annulus steady state solution, the linear stablity demarcation point can be pinpointed with the cost of a few steady state analysis, and a full-annulus time-accurate unsteady calculation can thus be avoid. This methodology enables a quick parameter study to investigate the various rotating flow instability phenomenon such as rotating stall and rotating instability.

III. The nonlinear flow solver

The nonlinear flow solver used in this work is NutsCFD, an unstructured finite volume Reynolds-averaged Navier–Stokes solver capable of dealing with rotating frame reference and periodic boundary conditions. The solver features the use of the Newton–Krylov algorithm, which significantly enhances the efficiency and robsutness when computing turbomachinery flows at off-design conditions. Details of the solver can be found in ref and only general information of the solver theory is provided below.

A. Governing equations

The integral form of the governing equations in a relative frame of reference with a constant angular velocity of ω is

$$\frac{d}{dt}\int_{\Omega_r} \mathbf{W} dV + \oint_{\partial\Omega_r} (\mathbf{F}_c^r - \mathbf{F}_v) dS + \int_{\Omega_r} \mathbf{F}_\omega dS = 0,$$

where $\mathbf{W}$ are the conservative variables $[\rho,\ \rho\mathbf{u},\ \rho E]^T$. The absolute and relative convective fluxes, $\mathbf{F}_c$ and $\mathbf{F}_c^r$, the viscous flux $\mathbf{F}_v$, and the additional flux due to rotation, $\mathbf{F}_\omega$, are defined as

$$\mathbf{F}_c = \begin{bmatrix} \rho\mathbf{u}\cdot\mathbf{n} \\ \rho\mathbf{u}\mathbf{u}\cdot\mathbf{n} + p\mathbf{n} \\ \rho H\mathbf{u}\cdot\mathbf{n} \end{bmatrix},\ \mathbf{F}_c^r = \mathbf{F}_c - (\mathbf{u}_{rot}\cdot\mathbf{n}) \begin{bmatrix} \rho \\ \rho\mathbf{u} \\ \rho E \end{bmatrix},\ \mathbf{F}_v = \begin{bmatrix} 0 \\ \tau\cdot\mathbf{n} \\ \mathbf{u}\cdot\tau\cdot\mathbf{n} + \kappa\mathbf{n}\cdot\nabla T \end{bmatrix},\ \mathbf{F}_\omega = \begin{bmatrix} 0 \\ \rho\boldsymbol{\omega}\times\mathbf{u} \\ 0 \end{bmatrix},$$

with $\mathbf{u}_{rot} = \boldsymbol{\omega}\times\mathbf{x}$. When ω is set to zero, a solver in the non-rotating reference frame is recovered.4

Turbulence is modeled using the negative Spalart–Allmaras (SA-neg) model [1]. Compared to the original SA model [1], this avoids the clipping of the turbulent variable to a non-negative value which potentially prevents the full convergence of the nonlinear solver. The turbulence equation is discretized using the first-order accurate upwind scheme [2].

B. Spatial discretization

The governing equations are discretized using the method of lines and thus the spatial and temporal discretizations can be treated separately. The governing equations for the steady-state solution $\mathbf{W}$ is

$$\mathbf{R}(\mathbf{W}) = \mathbf{0}, \tag{1}$$

where $\mathbf{R}$ is the sum of fluxes and source terms associated with each control volume. Suppose control volume i has N flux faces with area S_{ik} for $k = 1, 2, \ldots, N$. R_i then is

$$R_i(\mathbf{W}) = \sum_{k=1}^{N} (\mathbf{F}_c^r - \mathbf{F}_v) S_{ik} + \mathbf{F}_\omega V_i,$$

where V_i denotes the volume. The computation of the convective flux $\mathbf{F}_c^r$ is based on a modification of the Roe flux scheme to account for the relative reference frame that is rotating with a constant angular velocity; while the viscous flux $\mathbf{F}_v$ is the same as in the stationary reference frame.

C. Temporal discretization

The Newton method solves the steady-state nonlinear equation (1) iteratively as

$$\mathbf{W}^{n+1} = \mathbf{W}^n + \beta\Delta\mathbf{W}$$

until convergence is reached, i.e., $\|\mathbf{R}(\mathbf{W})\| = 0$, where $\Delta\mathbf{W}$ is the solution to the linear system of equations

$$\frac{\partial \mathbf{R}}{\partial \mathbf{W}}\Delta\mathbf{W} = -\mathbf{R}(\mathbf{W}^n)$$

The under-relaxation factor β is obtained using a line search.

Once the spatial discretization, $\mathbf{R}(\mathbf{W}^n)$, is established, there are three main steps to complete a Newton update step, namely, (i) forming the Jacobian matrix, (ii) solving the large sparse linear system of equations, and (iii) finding a step size β and update the nonlinear flow solution. To form the Jacobian matrix, automatic differentiatino tool Tapenade is used, together with graph coloring tool Colpack. By executing the foward-differentiated residual subroutine for a subsets of nodes with the same color, the Jacobian matrix is calculated. The resulting large sparse linear system of equations is solved using GMRES right-preconditioned by the incomplete LU factorization with zero fill-in.

IV. Global linear stability analysis via eigenmode decomposition

A. Global linear stability analysis

A nonlinear dynamic system, e.g., the discretised NS equation discretized using the method of lines, has the form

$$Vol\frac{d\mathbf{u}}{dt} = -\mathbf{R}(\mathbf{u})$$

where $\mathbf{u}$ is the time-varying flow variable and $\mathbf{R}(\mathbf{u})$ is the nonlinear residual representating the spatial discretization. Vol is a diagonal matrix with the volume of each dual cell on its diagonal. This term can be eliminated by redefining $\mathbf{R}(\mathbf{u})$ by applying volume scaling to it. The governing equation of the dynamic system then becomes

$$\frac{d\mathbf{u}}{dt} = -\mathbf{R}(\mathbf{u})$$

Assuming a steady state solution $\mathbf{u}_0$ (equilibrium point of the dynamic system) exists, and the time-varying flwo variable can be decomposed as the steady and the unsteady part

$$\mathbf{u} := \mathbf{u}_0 + \tilde{\mathbf{u}}$$

and the governing equation becomes

$$\frac{d\tilde{\mathbf{u}}}{dt} = A\tilde{\mathbf{u}}$$

where A is the negative Jacobian $A := -\dfrac{\partial \mathbf{R}}{\partial \mathbf{u}}$.

In order to use the eigen model decomposition approach, suppose the system matrix has right eigenvectors

$\{\mathbf{v}_i, \mathbf{v}_2, ..., \mathbf{v}_N\}$, which forms the matrix V as its colum vectors. Matrix A can then be factorized as

$$A = V\Lambda V^{-1}$$

where the diagonal matrix Λ has the eigenvalues on the matrix A as its diagonal elements. Decomposing the unsteady part $\tilde{\mathbf{u}}$ in the eigen modal space, it can be expressed as a linear combination of all eigenvectors with coordinates η

$$\tilde{\mathbf{u}} = V\eta$$

Substituting the $\tilde{\mathbf{u}}$ in the governing equation using the eigen modal decomposition, it becomes

$$\frac{d\eta}{dt} = \Lambda\eta$$

All variables are decoupled now and it can be written as

$$\frac{d\eta_i}{dt} = \lambda_i\eta_i \quad \forall i$$

For the linear system to be stable, the sufficient and necessary condition is that all eigenvalues has a negative real part, i.e., $\text{real}(\lambda_i) < 0, \forall i$.

B. Numerical implementation of eigenanalysis

In practice, performing the global linear stability analysis as described above is a standard procedure involving three steps: (i) find an equilirium point $\mathbf{u}_0$; (ii) linearize the nonlinear residual and form the Jacobian matrix A, and (iii) perform eigenanalysis and find Λ and V. Step (i) is simply running the steady state flow solver until a steady state solution is found. Step (ii) is a by-product of the nonlinear flow calculation using the NK method, i.e., store away the Jacobian matrix at the final Newton step. Step (iii) is a bit more involved for high dimensional problems.

For eigenmode computations, the implicitly restarted Arnoldi method proposed by Sorensen [3] and implemented in the ARPACK library [4], is used in combination with the NutsCFD solver. Shift-and-invert spectral transformation is applied to converge to wanted parts of the eigenspectrum, and critical is therefore the robust solution of many linear systems of equations. Key to efficiently solving the arising large sparse linear system of equations is the deflated Krylov subspace solver GCRO-DR [5]. Compared with the more commonly used GMRES solver [6], GCRO-DR is both more CPU time and memory efficient, especially as the system matrix condition worsens, as demonstrated in [7, 8].

V. Results

A. Laminar flow around a two-dimensional circular cylinder

Eigenvalue analysis is performed for the canonical case of the laminar flow around a circular cylinder with the Reynolds number in the range between 40 and 100. The computational domain is a circular cylinder centered at the origin with a diameter of $D = 10^{-5}$ and the farfield is a circle with a diameter of $100D$. The left half of the outer circle is set to 'farfield' boundary condition with a incoming flow of Mach 0.2 in the x-direction, a static pressure of 101325 Pa and and a temperature of 288.15 K. The right half ot he circle is set to 'pressure-outlet' boundary condition, with a constant pressure of 101325 Pa. The computational domain is meshed with quadrilateral elements, with a total of 29600 grid points. The density is 1.225 kg/m^3. The dynamic viscosity is varied in order to achieve a particular Reynolds number.

1. Steady state calculation

The steady state flow is obtained by either using an implicit solution method in Fluent (version 19.2) or by resorting to the Newton-Krylov algorithm in NutsCFD, despite the fact that the flow is physically unsteady under this condition. The Mach number contour of the NutsCFD calculation is shown in Fig. 1.

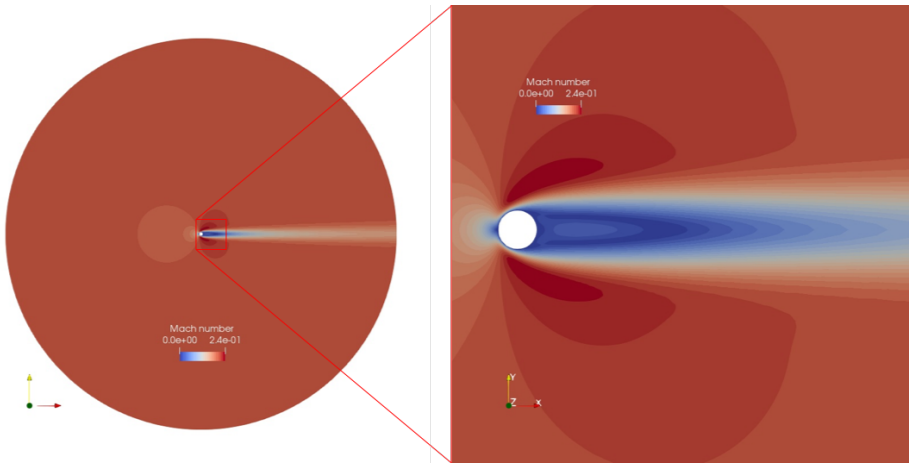

Fig. 1 Mach number contour plot of the calculation results by NutsCFD for Re = 55.

To compare the Fluent and NutsCFD results quantitatively, the velocity-x behind the cylinder as well as the pressure coefficient along the cylinder surface are compared in Fig. 2 and very good agreement can be found.

2. Unsteady calculation

Experimental results show that the laminar flow around the cylinder becomes unsteady for Re above a critical value (around 47). To study this phenomenon, unsteady flows for $Re = 55$ and $Re = 40$ are performed using NutsCFD. First, for both conditions, a steady state flow solution is obtained by converged the residual to machine error. For $Re = 55$, the

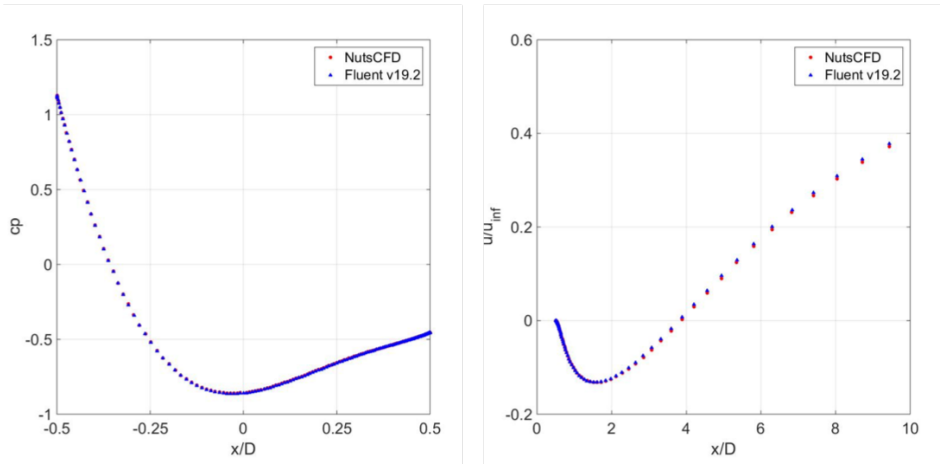

Fig. 2 Comparison between Fluent and NutsCFD calculation results for velocity-x along the center line behind the cylinder (left) and pressure coefficient along the cylinder surface (right).

unsteady simulation is run with the steady state as initial condition. A BDF2 second-order implicit dual-time-stepping method is used with the physical time step set to $10^{-8} sec$, that is, $0.01 ms$, and the inner loop is solved with a CFL of 1000 and maximum 5 iterations. Roughly two orders of magnitude of residual drop is achieved for the inner loop. From Fig. 3, it can be seen that after around $100 ms$, the lift coefficient starts to grow and eventually reaches a saturated limit cycle at around $130 ms$. On the contrary, running unsteady simulation with a fully converged steady state for $Re = 40$ does not lead to unsteadiness. To probe the flow at $Re = 40$ further, a disturbance is introduced into the flow from the farfield by setting the incoming flow direction to vertical for one time step and switching it back to the horizontal direction, and then continue the unsteady run. The lift coefficient shows a transient response but eventually slowly delays to zero. These two sets of lift coefficient signals are plotted in Fig. 3 in both linear and logrithm scales. The logrithmic plot on the right clearly shows an exponential growth and decay for $Re = 55$ and $Re = 40$, respectively.

3. Eigenanalysis

An eigenvalue analysis is performed for the steady state solution calculated in NutsCFD. After converging the steady state solver to machine error ($tol = 10^{-14}$), the exact Jacobian matrix based on the 2nd-order spatial accuracy is calculated and output to file. The sparse matrix is read into Matlab and eigs is used to compute a subset of the eigenvalues, with the aim of finding the (hopefully one) unstable mode. To minimize the computational effort, 10 eigenvalues/vectors are computed for matrices with different shifts of 0, i, $2i$, $3i$, $4i$, $5i$. All the eigenvalues, 60 in total and with some duplicated, are plotted in Fig. 4. It can be seen that there is one eigenvalue that is on the right side of the imaginary axis, indicating there is one unstable mode. In the meantime, from the time-domain simulation, one can extract from the lift-coefficient signal that the flow is linearly growing with a growth rate of 0.123 and oscillating with a circular frequency of 4.94 rad/s. This mode is plotted along with the spectrum and it can be seen that this mode also

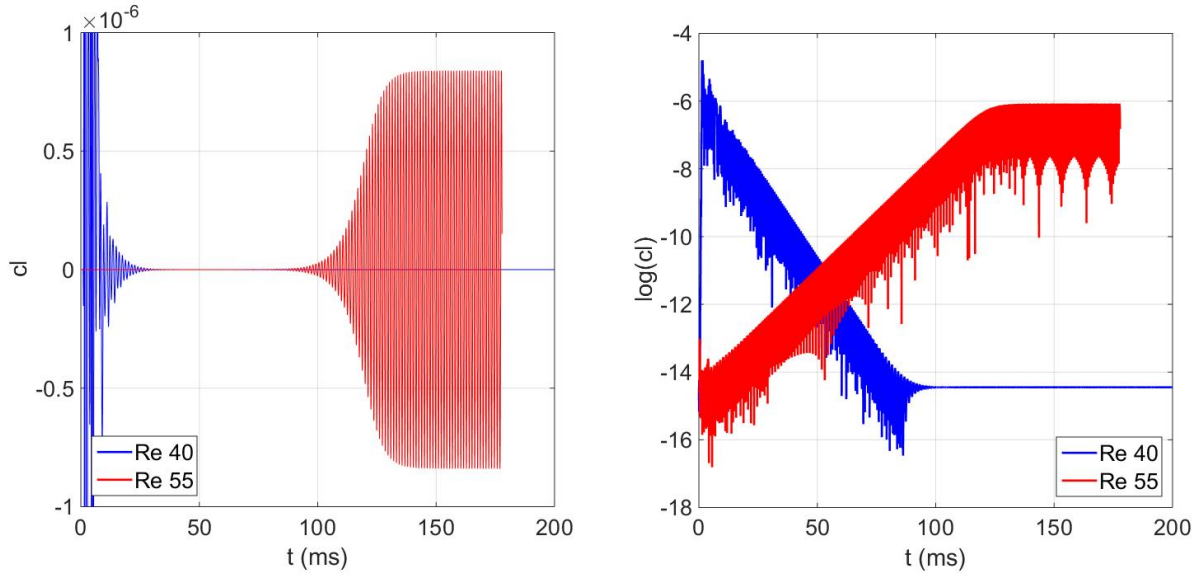

Fig. 3 Lift coeffient histogram for $Re = 55$ and $Re = 40$.

overlaps with the unstable eigenvalue from the eigenanalysis.

The eigenanalysis not only generates the eigenvalues but also the eigenvectors associated with each eigenvalue. For the unstable mode, the real part of the density, x/y momentum and energy component of the unstable eigenvector is shown in Fig.5.

add the eigenvector to the steady state solution to imitate the unsteady snapshot.

B. Transonic flow for an isolated rotor row (quasi-3D analysis)

NutsCFD is used to analyze the performance of the first stage rotor (NASA Rotor 67) of a two stage transonic fan designed and tested at the NASA Glenn center [9]. Its design pressure ratio is 1.63, at a mass flow rate of 33.25 kg/sec. The NASA Rotor 67 has 22 blades with tip radii of 25.7 cm and 24.25 cm at the leading and trailing edge, respectively, and a constant tip clearance of 1.0 mm. The hub to tip radius ratio is 0.375 at the leading edge (TC = 0.6% span) and 0.478 at the trailing edge (TC = 0.75% span). The design rotational speed is 16,043 RPM, and the tip leading edge speed is 429 m/s with a tip relative Mach number of 1.38.

As a first step, the analysis is performed on the surface of revolution taken at approximately 50% of the blade height. The three-dimensional mesh has one cell in the radial direction.

1. Steady state calculation

Steady state analysis is performed for both the single-passage and whole-annulus configurations. In order to obtain the steady state solutions for the whole annulus, which presumably is identical for each blade passage, we first compute

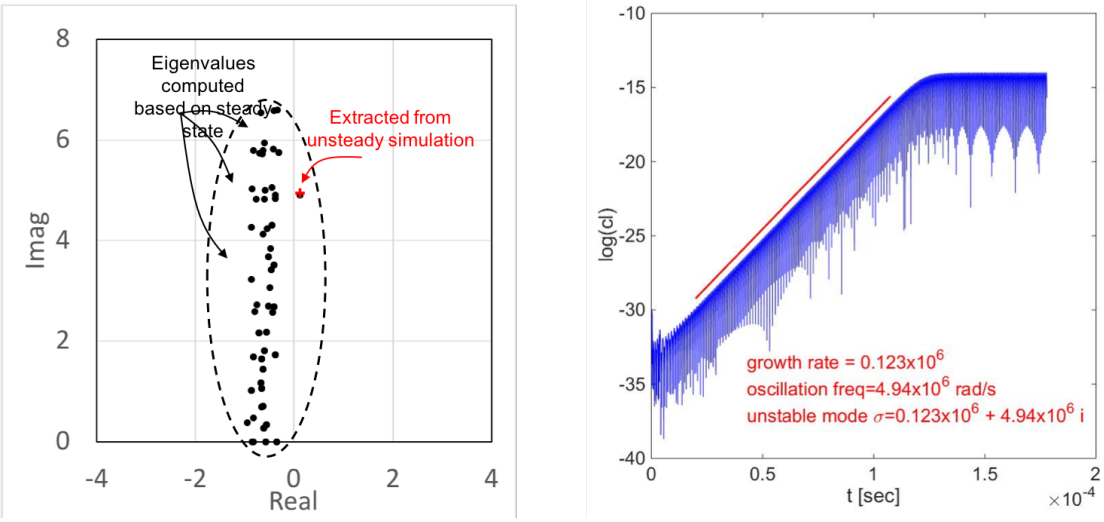

Fig. 4 Eigenspectrum from the steady state eigenvalue analysis compared with the linearly destabiling unsteady simulation for $Re = 55$.

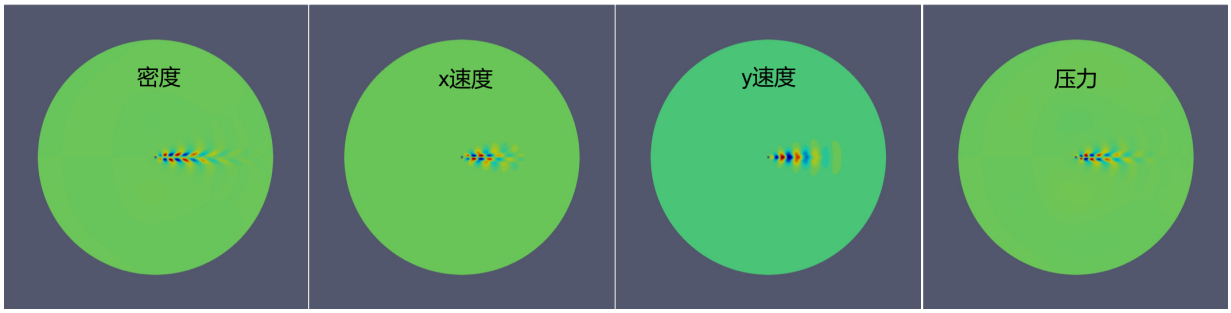

Fig. 5 Real part of the density, x/y momentum, energy components of the unstable eigenmode for $Re = 55$.

the steady state solution for one passage with rotatioal periodicity, and then copy the solution to the whoe annulus using rotational transformation. The pressure ratio and efficiency are shown in Fig. 6 which is produced by incrementally raising the back pressure from the inlet total condition. It can be seen that there is small difference (mainly efficiency) between the single-passae and whole-annulus results, which is due to the minor discrepancy of the spatial discretization at the periodic boundaries for single passage calculation.

The flow solution using either single passage or whole annulus is shown in Fig. 7, which visually shows that the solutions are not distinguishable.

2. Eigenanalysis

For each whole-annulus steady state solution, eigenanalysis is performed using the Jacobian matrix output from the NutsCFD solver once the steady state calculation has fully converged. Since the rotational speed for the rotor is 16,043 RPM, the Jacobian matrix is scaled by a factor of $1/(2\pi \times 16,043/60) \approx 1/1680$, so that all frequencies involved in this computation is reduced by the rotor angular frequency. This is done due to the pre-knowledge that rotating stall cells

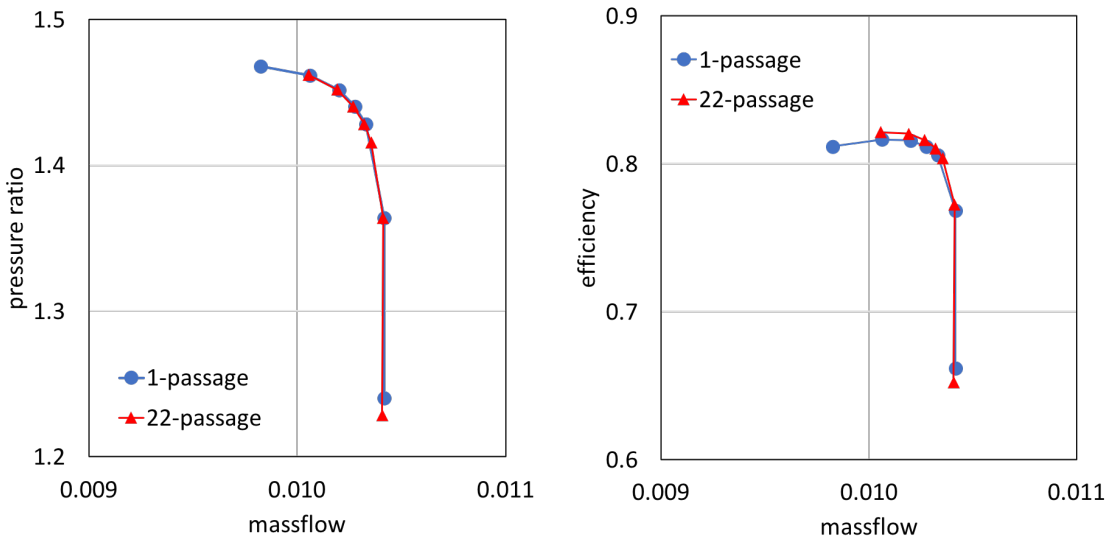

Fig. 6 Q3D performance for rotor67 at 50% blade height with either single passage or whole annulus (22 passages).

move with speed of the same order of magnitude.

Shown in Fig. **??** is a subset of the eigenvalues that are near the imaginary axis, which presumally are most likely to be unstable. The eigs function in Matlab is used with various imaginery shifts to compute interior eigenvalues. The ones that are suspecious of crossing the imaginery axis are shown. A zoomed view of the eigenvalues reveals that there are a total of five that have positive real parts, i.e., unstable.

The pressure component of the eigenvector corresponding to one eigenvalue is visualized to the right of Fig. 8. The circumferential synchronized shock oscillation can be easily spotted. Eigenvectors of other unstable mode are similar, except with different circumferential variation, which can further be attributed to different nodal diameters, which varies from 5 to 9, continuously, from eigenvalues 1 to 5.

The eigenvector labelled with '1' is visualized in Fig. 11 with both the real and imaginary parts. The synchronized circumferential shock oscillation can be seen. To analyze the spatial modes, data along the intersecting curve is taken (marked at the red line in Fig. 11). This is done for each of the 11 modes, and a few of them are shown in Fig. **??**. It is clear that the n-th eigenvector corresponds to a rotating pattern with nodal diameter n.

A more involved data processing reveals that the perturbation pattern, for every eigenvector, is a travelling wave that rotates in the opposite direction of the motion of the rotor, and with a speed a fraction of the shaft rotating speed. This relative rotating speed can be calculated using the imaginary of the eigenvalue and the nodal diameter of the perturbation pattern as $\frac{\omega}{\omega_{shaft}}\frac{1}{ND}$. In experiment, instrumentation for detecting rotating instability is usually sensors installed on the stationary casing and the speed of the rotating cells is also measured in the absolute reference frame. In the absolute

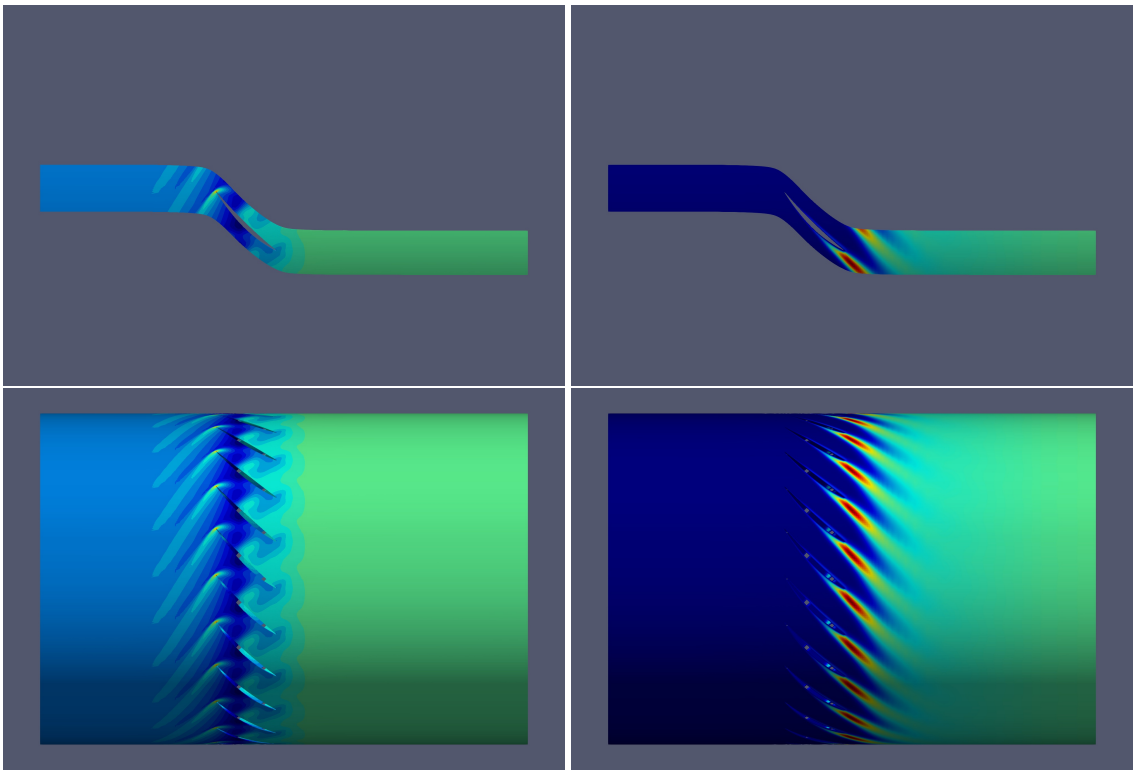

Fig. 7 Pressure (left) and SA variable (right) contours for single passage (top) and whole annulus (bottom) calculations.

reference frame, the cell rotating speed is calculated as

$$U_{cellRotating} = 1 - \frac{\omega}{\omega_{shaft}} \frac{1}{ND}. \tag{2}$$

Applying this formula to each of the 11 eigenmodes leads to the correlation between the nodal diameter and the perturbation rotating speed.

VI. Conclusion

Acknowledgements

References

[1] Allmaras, S. R., and Johnson, F. T., "Modifications and clarifications for the implementation of the Spalart-Allmaras turbulence model," *Seventh international conference on computational fluid dynamics (ICCFD7)*, 2012, pp. 1–11.

[2] Langer, S., "Agglomeration multigrid methods with implicit Runge–Kutta smoothers applied to aerodynamic simulations on unstructured grids," *Journal of Computational Physics*, Vol. 277, 2014, pp. 72–100.

[3] Sorensen, D. C., "Implicit application of polynomial filters in a k-step Arnoldi method," *SIAM journal on matrix analysis and*

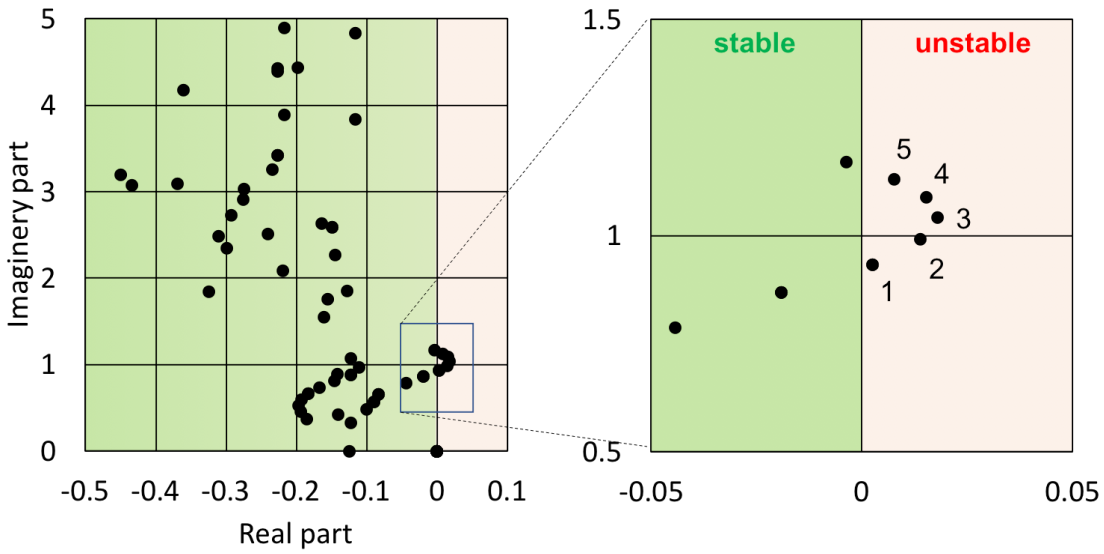

Fig. 8 Spectrum for back pressure 18kpa.

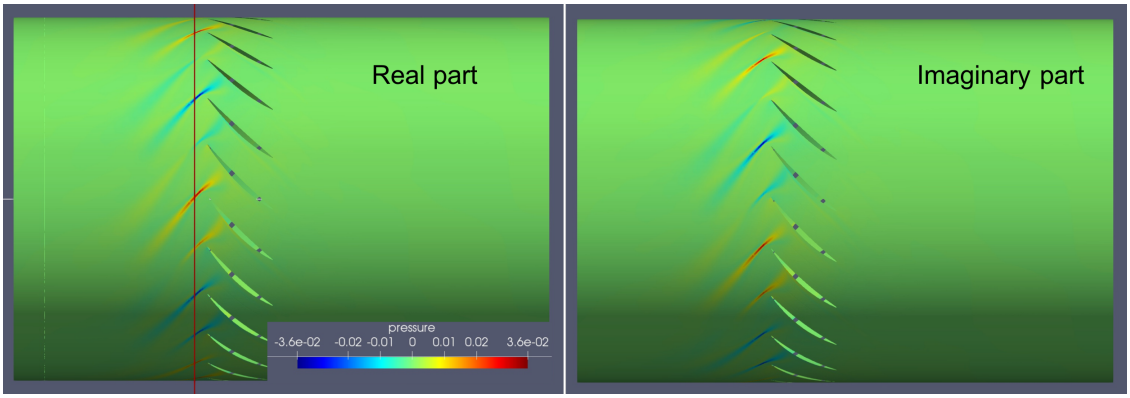

Fig. 9 Eigenvector 5 visualized using the real and imaginary parts of the pressure.

applications, Vol. 13, No. 1, 1992, pp. 357–385.

[4] Lehoucq, R. B., Sorensen, D. C., and Yang, C., *ARPACK users' guide: solution of large-scale eigenvalue problems with implicitly restarted Arnoldi methods*, Vol. 6, SIAM, 1998.

[5] Parks, M., de Sturler, E., Mackey, G., Johnson, D., and Maiti, S., "Recycling Krylov subspaces for sequences of linear systems," *SIAM Journal on Scientific Computing*, Vol. 28, No. 5, 2006, pp. 1651–1674.

[6] Saad, Y., and Schultz, M. H., "GMRES: A generalized minimal residual algorithm for solving nonsymmetric linear systems," *SIAM Journal on scientific and statistical computing*, Vol. 7, No. 3, 1986, pp. 856–869.

[7] Xu, S., Timme, S., and Badcock, K., "Enabling off-design linearised aerodynamics analysis using Krylov subspace recycling technique," *Computers & Fluids*, Vol. 140, 2016, pp. 385–396.

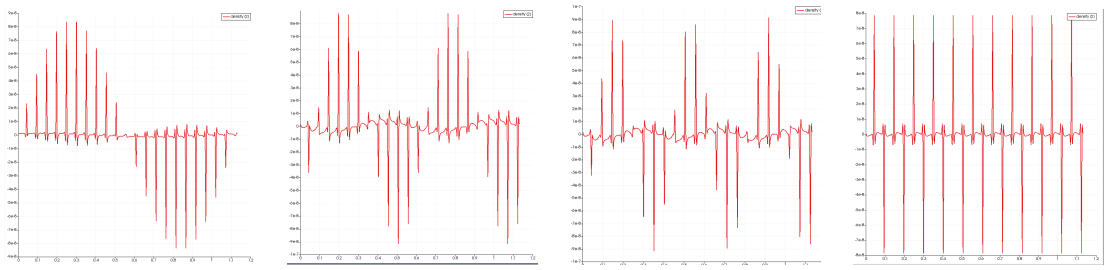

Fig. 10 The circumferential distribution for the real part of the pressure component of the 1st, 2nd, 3rd and 11th eigenvectors.

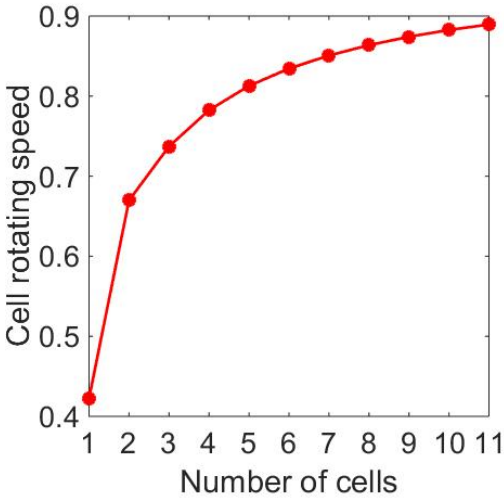

Fig. 11 The cell rotating speed v.s. the number of cells (nodal diameter of the perturbation pattern).

[8] Xu, S., and Timme, S., "Robust and efficient adjoint solver for complex flow conditions," *Computers & Fluids*, Vol. 148, 2017, pp. 26–38.

[9] Strazisar, A. J., Wood, J. R., Hathaway, M. D., and Suder, K. L., "Laser anemometer measurements in a transonic axial-flow fan rotor," 1989.